Breast cancer cells alter the dynamics of stromal fibronectin-collagen interactions

Karin Wang[1,2,3], **Fei Wu**[1], **Bo Ri Seo**[2,4], **Claudia Fischbach**[2], **Weisi Chen**[1], **Lauren Hsu**[1], and **Delphine Gourdon**[1,5,*]

[1]Department of Materials Science and Engineering, Cornell University, Ithaca, NY 14583, USA

[2]Nancy E. and Peter C. Meinig School of Biomedical Engineering, Cornell University, Ithaca, NY 14583, USA

[5]Department of Physics, University of Ottawa, Ottawa, ON K1N 6N5, Canada

Abstract

Breast cancer cells recruit surrounding stromal cells, such as cancer-associated fibroblasts (CAFs), to remodel their extracellular matrix (ECM) and promote invasive tumor growth. Two major ECM components, fibronectin (Fn) and collagen I (Col I), are known to interact with each other to regulate cellular behavior. In this study, we seek to understand how Fn and Col I interplay and promote a dysregulated signaling pathway to facilitate tumor progression. Specifically, we investigated the evolution of tumor-conditioned stromal ECM composition, structure, and relaxation. Furthermore, we assessed how evolving Fn-Col I interactions gradually affected pro-angiogenic signaling. Our data first indicate that CAFs initially assembled a strained, viscous, and unfolded Fn matrix. This early altered Fn matrix was later remodeled into a thick Col I-rich matrix that was characteristic of a dense tumor mass. Next, our results suggest that this ECM remodeling was primarily mediated by matrix metalloproteinases (MMPs). This MMP activity caused profound structural and mechanical changes in the developing ECM, which then modified vascular endothelial growth factor (VEGF) secretion by CAFs and matrix sequestration. Collectively, these findings enhance our understanding of the mechanisms by which Fn and Col I synergistically interplay in promoting a sustained altered signaling cascade to remodel the breast tumor stroma for invasive breast tumor growth.

*Corresponding author: Professor Delphine Gourdon, Department of Materials Science and Engineering, Cornell University, 327 Bard Hall, Ithaca, NY 14853-1501, USA, dg434@cornell.edu, dgourdon@uottawa.ca.

[3]Molecular and Integrative Physiological Sciences, Department of Environmental Health, Harvard T.H. Chan School of Public Health, Boston, MA 02115, USA (present address)

[4]Bioengineering, John A. Paulson School of Engineering and Applied Sciences, Harvard University, Cambridge, MA 02138, USA (present address)

---

1. Introduction

Particular focus has been placed on studying the altered extracellular matrix (ECM) during tumorigenesis, as it provides biochemical and biomechanical cues that alter cellular functions [1,2]. Fibronectin (Fn), a major ECM glycoprotein, regulates cell signaling and behavior in both physiological and pathological conditions. Fn is a mechanotransducer protein: cell-induced conformational changes affect cell adhesion and growth factor binding [3]. Cancer cells, unable to assemble their own Fn matrix, signal surrounding cells in the stroma such as cancer-associated fibroblasts (CAFs) to up-regulate Fn [4]. These tumor-secreted factors mediate the early stromal assembly of a thick, dense, and stretched Fn matrix comprising highly unfolded molecules [5]. This altered Fn matrix not only exhibits increased stiffness and viscosity, but also mediates enhanced pro-angiogenic signaling [6]. Collagen I (Col I) is another prominent ECM protein with multiple contributions to tumorigenesis [7,8]. Col I deposition is primarily dependent on previously assembled Fn matrices [9–12]. Therefore, assessing how Fn-Col I interactions are altered during tumorigenesis is critical to our understanding of tumor stroma modifications that mediate invasive tumor growth.

In this study, we seek to elucidate the dynamics of tumor conditioned (TC)-ECM assembly. Specifically, we (i) assessed composition, topology, conformation, and relaxation of the composite TC-ECM (Fn and Col I) over time, (ii) evaluated how matrix metalloproteinase (MMPs) activity contributed to altered TC-ECM evolution, and (iii) determined subsequent changes in pro-angiogenic activity by quantifying both secreted and matrix-bound vascular endothelial growth factor (VEGF) in TC-ECM conditions.

2. Results and Discussion

2.1. Topological and conformational evolution of the tumor-conditioned (TC) matrix

ECM assembled by control (c−) and TC-pre-adipocytes, a model of cancer-associated fibroblasts in the peritumoral region, were cultured over a period of 9 days to evaluate the deposition and remodeling of both Fn and Col I. Previous studies have shown that these cells initially deposit a TC-Fn matrix that exhibits altered structural [5] and mechanical properties [5,6]. We sought to understand how the altered materials properties of the TC-Fn matrix propagate over time: more specifically, how these early structural changes to Fn, affect downstream Col I deposition and contribute to stromal changes during tumorigenesis.

Immunofluorescence of c- and TC-ECM portrayed an initial (Day 1) ECM composed primarily of Fn (Figure 1a; Day 1 & SI Figure 1). Early TC-Fn fibers were thinner than c-Fn fibers (Figure 1b; **Fn** Day 1: 0.84 μm vs. 0.87 μm; $p < 0.05$), which is likely due to higher strain (higher linearity) of TC-Fn fibers (Figure 1c; **Fn** Day 1: 0.91 vs. 0.88). These TC-Fn fibers also comprised more unfolded Fn molecules, as indicated by the lower FRET intensity

ratios (FRET IR) (Figure 1d,e; **FRET maps**: low FRET IR color-coded blue and high FRET IR color-coded red; **FRET** Day 1: 2.303 vs. 2.566; $p < 0.0001$). The initial structural changes to the TC-Fn matrix likely modified cell-Fn and Fn-Col interactions by exposing/disrupting cryptic binding sites on Fn [13–15]. Furthermore, subtle increases in fiber diameters and unfolding of Fn molecules within fibers, suggest that ligand density on TC-Fn fibers may have increased either via fiber surface area or fiber volume [14]. However, as the resolution of our confocal microscopy experiments is around 200 nm, thinner fibers–which could be as thin as 12 nm [16] – may have been missed, and may have led us to overestimate fiber diameter.

An established Fn matrix is generally required for the assembly of other ECM proteins such as fibrillins [17] and collagens [9]. However, one study reports collagen deposition in the absence of Fn through transforming growth factor-β1 (TGF-β1) compensation [18], which may explain the presence of sparse and linearized TC-Col I fibers found at Day 1 (Figure 1a; **Col I** Day 1: 0.79 μm vs. 0.79 μm; Figure 1c; **Col I** Day 1: 0.89 vs. 0.85). TGF-β1 was previously shown to be a major component of the TC media used to pre-condition the pre-adipocytes in our study [5]. Additionally, Fn and procollagen have been found to co-localize within similar cellular compartments of fibroblasts during secretion [19], which may also contribute to the occasional co-assembly of Fn and Col I in early c-ECMs (Figure 1a; Day 1, white arrowheads).

By Day 5, numerous thin TC-Fn fibers overlapped with thick bundles of TC-Col I fibers (Figure 1a white regions of fibers indicate co-localization of Fn and Col I). However, in c-ECM, only fragmented/digested Fn and thin Col I fibers were present. By Day 9, more differences arose between c- and TC-ECM (Figure 1a; Day 9). The TC-Fn matrix was replaced by a rich Col I network exhibiting thick TC-Col I fibers (Figure 1b; **Col I** Day 9: 0.9 μm vs. 0.76 μm; $p < 0.0001$). The remaining TC-Fn fibers were consistently thicker (Figure 1b; **Fn** Day 9: 0.75 μm vs. 0.66 μm) and more unfolded than their control counterparts (Figure 1d,e; **FRET** Day 9: 2.552 vs. 2.975; $p < 0.0001$). Overall, higher FRET IR was measured in both c- and TC-Fn fibers at later times, when Col I was predominant in the ECM (Figure 1e; Day 9 vs. Day 1). This effect can be attributed to the concomitant binding of Col I to $FnI_6FnII_{1-2}FnI_7$ and FnI_{8-9} (gelatin binding domain of Fn), which maintains Fn in a more relaxed/compact conformation by stabilizing the kink between FnI_7 and FnI_8 [12,20].

Interestingly, the initially higher linearity of both TC-Fn and TC-Col I fibers decreased at Day 5 (Figure 1c; **Fn** Day 5: 0.87 vs. 0.89; **Col I** Day 5: 0.82 vs. 0.85; $p < 0.05$) before converging towards values similar to that of control fibers at Day 9 (Figure 1c; **Fn** Day 9: 0.88 vs. 0.88; **Col I** Day 9: 0.88 vs. 0.88). This convergence to steady-state (ideal) linearity values suggests that individual fiber strain (and associated long-range force transmission between cells) [21,22] may be crucial in the developing ECM, but irrelevant in the mature ECM present in bulk tissues once Fn-Col I synergy is well established.

Also, previous single Col I fiber mechanical characterization reports a tensile elastic modulus of 123 MPa [23], which is far higher than the ~3.5 MPa value measured on Fn fibers when stretched up to 700% [24]. Therefore, the role of thick and stiff Col I fibers in

mature ECMs is likely to bear most of the microenvironmental tension. Thus enabling initially strained Fn fibers to relax, and consequently decrease the amount of unfolded modules present in individual fibers. TC-Fn's more relaxed conformations within the mature ECM would then lead to enhanced Col I deposition [12] and cellular migration [25] to promote a dysregulated feedback loop for tumor progression.

Previous studies have shown that Col I requires the initial assembly of a Fn matrix template for subsequent fibrillogenesis [9,10]. Collectively, our data suggest that the altered morphology and conformation of early deposited TC-Fn fibers lead to the assembly of an altered Col I matrix in the tumor stroma. Later, these mature dysregulated Col I fibers are only able to partially stabilize Fn against unfolding (as indicated by the persistent lower FRET IR in TC-Fn fibers at Day 9). Consequently, once altered Col I is assembled into mature ECM, its bulk tissue topology may be the driving force of altered tumor stroma mechanotransduction.

2.2. Mechanical relaxation of TC-Fn fibers

In the viscoelastic and composite ECM, individual Fn fibers are themselves highly viscoelastic [24,26,27] and heterogeneous elements that consist of several coexisting molecular conformations (ranging from compact/relaxed to extended/unfolded) [28,29]. During ECM evolution, Fn fibers are assembled, stretched and/or cleaved. Fn fibers undergo multiple cycles of dynamical strain and relaxation, as cells reorganize and remodel the entire fibrillar network (SI movies). In agreement with previous studies of Fn fiber reorganization [30], we observed that globular Fn patches were either translocated to pursue Fn fiber extension or digested after fiber breakage. We first assessed Fn fiber kinetics by tracking individual fibers and by measuring the decay of their length after breakage over time to obtain mean retraction velocities. All c- and TC-Fn fiber retraction velocities (μm/min) decreased significantly over time (Figure 2a: TC-Fn: Day 1 = 0.33 μm/min; $p < 0.05$. Day 5 = 0.21 μm/min; $p < 0.0001$. Day 8 = 0.22 μm/min; $p < 0.001$; c-Fn: Day 5 = 0.2 μm/min; $p < 0.0001$. Day 8 = 0.21 μm/min; $p < 0.0001$) compared to the c-Fn fiber retraction velocity at Day 1 (0.57 μm/min). To determine single Fn fiber relaxation more accurately, we next fitted our fiber data to single exponential decays and extracted individual relaxation times (SI Figure 2). Interestingly, our analysis revealed overall longer relaxation times, τ (min), for TC-Fn fibers than for c-Fn fibers (Figure 2b: TC-Fn: Day 1 = 21.8 min. Day 5 = 38.9 min. Day 8 = 45.4 min; c-Fn: Day 1 = 11.5 min; Day 5 = 14.3 min; Day 8 = 26.8 min). Additionally, as the ECM evolved from a sparse Fn matrix to a denser composite Fn-Col I network, longer relaxation times were measured for all Fn fibers.

Although we previously reported 2 different relaxation regimes (fast and slow) and longer relaxation times for TC-Fn at the matrix level [6], here we provide the first evidence, to our knowledge, of longer relaxations for TC-Fn at the fiber level. These new data suggest that the longer relaxation times observed at the matrix level in TC conditions [6] are mainly due to viscoelasticity. Solvent redistribution through the matrix pores, or poroelasticity, would lead to relaxation times on the order of a few seconds [31]. But conformational/structural changes in the Fn network, or viscoelasticity, would lead to relaxation times on the order of minutes. Additionally, our present results indicate that viscous changes are taking place not

only between but also within individual fibers comprising the TC matrix. This enhanced viscoelasticity of TC-Fn fibers may be attributed to a more rapid assembly/reorganization of these fibers into a deoxycholate-insoluble form [32], leading to inherent changes in the overlap and cross-linked arrangement of Fn molecules within fibers [33]. The misfolding would in turn affect Fn molecules' pathway to re-assemble into their native globular state [34], and the overall time Fn fibers take to unfold/refold properly [23]. Additionally, the thicker TC-Fn fibers may entrap more interstitial fluid within their core, which may slow down their individual dynamics [35,36]. Variability in fiber relaxation times may be due to mixed populations of Fn fibers analyzed (fibers located at both the leading edge and the rear edge of cells were monitored [37]) and/or to heterogeneous local tension in the network [38]. Finally, the presence of a concomitant Col I network [7,39] in the mature TC-ECM may induce additional noncovalent hindrance of Fn fiber kinetics over time [40]. Though Col I fibers were not noticeable in the SI movies, as only Fn was immunofluorescent, Col I fibers were present (Figure 1a and SI Figure 1). Whether it is co-localized or not, the dense network of thicker and stiffer Col I fibers, with its own viscoelastic properties [23], likely interferes with individual Fn fiber relaxation (friction, entanglement) [41].

Collectively, our results indicate that, besides being thicker and more unfolded, individual TC-Fn fibers are also more viscous than their control counterparts. Moreover, the longer relaxation times measured in TC samples increase as the ECM is developing. The enhanced viscosity in the ECM likely contributes to sustaining tumorigenesis by ensuring: (i) altered interplay with Col I and (ii) altered mechanosignaling to surrounding cells, over longer times.

2.3. Matrix metalloproteinase (MMP) contributions to altered TC matrix remodeling

Then, we sought to elucidate the evolution of the altered TC ECM. One mechanism that may play a role in physically remodeling the TC ECM is MMP activity. MMPs not only proteolytically digest ECM proteins [42,43], but also for example, render ECM proteins into bioactive fragments that could aid in proliferation [44]. Furthermore, MMPs may also have non-proteolytic functions in modulating a multitude of cellular behaviors such as migration [45]. As a means of assessing MMP contributions during TC-ECM remodeling in a holistic manner, a broad spectrum MMP inhibitor, Batimastat, was utilized in parallel experiments. Immunofluorescence of MMP inhibited (MI/) TC-ECM displayed a radically different distribution of Fn and Col I over time (Figure 3a) compared with that of TC-ECM in Figure 1a. MI/TC-ECM revealed a prevailing dense Fn network consisting of thick and aligned fibers (Figure 3b; **Fn** Day 1: 0.92 μm; $p < 0.01$ (c-Fn); $p < 0.0001$ (TC-Fn), Day 5: 0.88 μm; $p < 0.0001$ (c-Fn & TC-Fn), Day 9: 0.8 μm; $p < 0.0001$ (c-Fn); $p < 0.01$ (TC-Fn)). These data suggest that, when unable to degrade/remodel the previous ECM network, TC-cells utilize the previously assembled Fn as an underlying framework to pursue Fn deposition.

Although MI/TC-Fn fibers were under low/normal strain at Day 1 and 9, they were significantly more strained than TC-Fn fibers at Day 5 (Figure 3c; **Fn** Day 1: Day 1: 0.89, Day 5: 0.92; $p < 0.05$, Day 9: 0.87). MI/TC-Fn fibers were likely under different mechanical strains, as very few Col I fibers were present in the ECM to stabilize them against unfolding by cell traction forces. Indeed, the MI/TC-Col I fibers deposited were sparse and very thin

(Figure 3b; **Col I** Day 1: 0.78 μm, Day 5: 0.67 μm; $p < 0.0001$ (c-Fn & TC-Fn), Day 9: 0.84 μm; $p < 0.0001$ (c-Fn); $p < 0.001$ (TC-Fn)). MMP activity is likely critical for tumor stroma remodeling, in particular for TC-cells to proteolytically degrade and remodel TC-Fn, in order to expose Col I binding sites for downstream TC-Col I deposition. Specifically, MT-MMP1 (MMP 14), a major MMP inactivated by Batimastat, is essential for Fn cleavage [46] and endocytosis [47]. MT-MMP1 is also implicated in collagen turnover during normal tissue homeostasis [48]. The few MI/TC-Col I fibers present were nearly as strained (linear) as c-Col I fibers (Figure 3c; **Col I** Day 1: 0.83, Day 5: 0.86, Day 9: 0.89). Similarly to c- and TC- fibers, the linearity of all MI/ fibers converged at Day 9, which suggests an optimal individual fiber strain in the mature ECM, even when inhibited MMP activity restrains ECM remodeling.

Together, our inhibition studies reveal the crucial role of MMP activity during tumor progression in remodeling stromal Fn to enable subsequent Col I fibrillogenesis. The presence of a predominantly highly strained Fn matrix also confirms that mechanoregulation of Fn-Col I interaction (via exposure of Fn-binding sites for Col I) is possibly responsible for Col I fibrillogenesis. It is unlikely that TGF-β1 plays a major role in Col I fibrillogenesis when Fn is present, as MMP- inhibited samples were all preconditioned and supplemented with TC medium containing TGF-β1 and very little Col I was assembled. However, other mechanisms of ECM remodeling, such as lysyl oxidase (LOX) or fibroblast activation protein (FAP) [7,49,50], which were beyond the scope of this study, may contribute to the impeded, but continued TC-ECM remodeling.

2.4. Proangiogenic secretion and growth factor sequestration during matrix evolution

MMP activity is complex. Not only does MMP activity induce physical remodeling of ECM fibers, but MMP activity has also been implicated in growth factor bioavailability and activation of vascular endothelial growth factor (VEGF) [51,52]. Thus, to understand the effect of ECM altered properties on growth factor secretion and matrix sequestration for tumor growth, both VEGF secretion by CAFs and VEGF immobilization to Fn fibers were quantified during TC-ECM remodeling. Altered fiber thickness, strain, and conformation of the TC-ECM may all alter cell binding and immobilization/bioavailability of VEGF. Cell population assessed by DNA quantification revealed no significant differences between c- and TC-cells (Figure 4a; **DNA** Day 1: 1.27 vs. 1; Day 5: 3.97 vs. 3.26; Day 9: 4.34 vs. 4.43). However, less DNA was measured in MMP inhibited samples (Figure 4a; **DNA** Day 1: 1.08, Day 5: 1.61; $p < 0.0001$ (TC-ECM & MI/TC-ECM), Day 9: 1.84 vs. 4.34; $p < 0.001$ (TC-ECM & MI/TC-ECM)). This decrease in cell population is likely due to alterations of Fn as it plays a major role in cell proliferation [53]. Interestingly, TC-VEGF secretion was overall lower than c-VEGF. And TC-VEGF secretion decreased significantly at later time points when TC-Fn fibers were evolving towards less strained and molecularly relaxed fibers due to the presence of Col I (Figure 4b; **VEGF** Day 1: 1.11 vs. 1, Day 5: 0.57 vs. 1.13, Day 9: 0.70 vs. 2.10; $p < 0.05$ (TC-ECM & c-ECM)).

In addition to numerous binding sites for cells and other ECM components, Fn possesses binding sequences for various growth factors, among which is the Hep2 domain for VEGF located on FnIII$_{12-14}$ [54]. To test whether VEGF preferentially immobilizes to TC-Fn, a

ratiometric analysis of immunofluorescently-labeled $VEGF_{165}$, normalized by 633-labeled Fn, was performed over time. Our ratiometric analysis revealed that, although less VEGF was immobilized on stretched and unfolded TC-Fn fibers than on c-Fn fibers at Day 1 and Day 5, the overall VEGF sequestered into TC-ECM increased significantly over time (Figure 4c; **Bound-VEGF** Day 1: Day 1: 0.88 vs. 1; $p < 0.001$, Day 5: 1.20 vs. 1.42; $p < 0.05$, Day 9: 1.66 vs. 1.16; $p < 0.01$ (TC-ECM & c-ECM)). These results suggest that the global decrease of VEGF secretion measured over time in TC conditions may be due to increased immobilization of VEGF to the TC-ECM while it gradually evolved towards a more relaxed collagen rich matrix [55–57].

Additionally, as MMP activity was inactivated, MI/TC-VEGF secretion drastically increased at Day 5 before decreasing back to nearly initial levels at Day 9 (Figure 4b; **VEGF** Day 1: 0.66; $p < 0.01$ (c- & TC-ECM), Day 5: 1.97; $p < 0.05$ (c-ECM); $p < 0.0001$ (TC-ECM), Day 9: 0.78; $p < 0.05$ (c-ECM)). However, MI/TC-bound VEGF levels remained low at Day 5 before increasing noticeably at Day 9 (Figure 4c; **Bound VEGF** Day 1: 0.82; $p < 0.001$ (c-ECM), Day 5: 0.74; $p < 0.001$ (c-ECM); $p < 0.001$ (TC-ECM), Day 9: 1.02; $p < 0.01$ (TC-ECM)). These data suggest that, in presence of a matrix comprising exclusively stretched/unfolded Fn at Day 5, the ratio between secreted and matrix-bound VEGF is very high. This difference is likely due to: (i) a switch from $\alpha_5\beta_1$ to $\alpha_v\beta_3$ integrins operated by CAFs to engage the surrounding highly strained ECM, which has been previously linked with enhanced VEGF secretion [6,58,59], and (ii) a strain-induced disruption of the Hep2 binding domain on Fn preventing direct VEGF binding [60]. Instead, when MI/TC-Fn fibers become less linear at Day 9, and more relaxed (Figure 2c), the ratio between secreted and matrix-bound VEGF decreases. Cells likely switch back to $\alpha_5\beta_1$ integrins to simultaneously engage the synergy site and the RGD loop located on the undisrupted $FnIII_{9-10}$ sequence, while VEGF can bind properly to the rescued (relaxed) Hep2 domain.

Note that, together with Fn conformation, both the global amount of Fn fibers and the fibers diameter could also directly affect the amount of sequestered (and secreted/soluble) VEGF. For example, at Day 9, although they exhibit similar linearity, TC-Fn fibers are thicker than c-Fn fibers. TC-Fn fibers thus expose more binding sites per unit volume, which could explain the higher levels of immobilized VEGF (and lower levels of soluble VEGF) measured in TC conditions with respect to control.

To gain insights into the mechanisms that direct the assembly of complex stromal ECM architectures and their potential role in tumor invasion, we probed the interplay between Fn and Col I fibers as they were assembled and remodeled by CAFs, in presence of breast tumor secreted factors. Our study indicates that CAFs initially assembled a viscous and stretched/unfolded Fn matrix, later remodeled into a dense predominantly Col I matrix. This MMP-mediated remodeling caused profound structural and mechanical changes in the developing stromal ECM. The altered ECM then modified pro-angiogenic signaling by altering both CAFs' secretion and ECM sequestration of VEGF over time. Collectively, our findings enhance our understanding of how Fn and Col I synergistically interplay in promoting either: (i) normal tissue formation (essential for tissue engineering and regenerative medicine), or (ii) a sustained altered signaling cascade to remodel the breast tumor stroma and facilitate downstream breast tumor invasion. The cell-mediated

mechanoregulation of structural ECM component interactions among each other and their associated matrix architectures (in both physiological and pathological environments), provides another example of how forces can impact the mechanobiology of ECM and thereby cell and tissue fate.

3. Experimental Procedures

3.1. Cell culture

3T3-L1 pre-adipocytes and MDA-MB-231 breast cancer cells (ATCC, VA) were cultured in Minimum Essential Medium (α-MEM) with 10% fetal bovine serum (FBS) and 1% penicillin-streptomycin (PS). Tumor soluble factors (TSF) were obtained from MDA-MB-231 cells cultured in α-MEM (1% FBS & 1% PS) for 24 hrs. 3T3-L1s were preconditioned with either control (c−) or normalized TSF (TC−) in α-MEM (1% FBS & 1% PS) for 3 days, before seeding 5×10^3 cells/0.8 cm^2 for immunostaining and conformational studies, or 25×10^3 cells/3.8 cm^2 for pro-angiogenic studies onto Fn-coated (30 μg/mL) Lab-Tek™ chambered coverglass (Thermo Scientific, MA) or 12-well plates (Corning, MA), respectively. Preconditioned cells were maintained in conditioning medium until 24 hrs before a timepoint (Day 1, 5, 9), and then switched to α-MEM (1% FBS & 1% PS) with Fn (50 μg/mL with 10% labeled Fn for conformational, fiber kinetics, or VEGF immobilization experiments). After 24 hrs, samples were fixed for FRET or immunostained imaging. For matrix metalloproteinase inhibition experiments, additional samples were supplemented with 20 μM Batimastat every other day (Millipore, MA).

3.2. Immunofluorescence

Nonspecific binding was blocked with PBS/1% SuperBlock (Thermo Scientific, MA) for 1 hr at room temperature before immunostaining for Fn (1:400 anti-mouse antibody) (Sigma-Aldrich, MO), Col I (1:100 anti-rabbit antibody) (EMD Millipore, MA), or $VEGF_{165}$ (1:100 anti-mouse antibody) (EMD Millipore, MA) overnight at 4°C. After washing with PBS (2x), samples were incubated with Alexa Fluor 647 goat anti-mouse (1:100) or Alexa Fluor 488 goat anti-mouse (1:100), Alexa Fluor 488 goat anti-rabbit (1:100), Alexa Fluor 568 Phalloidin (1:250), and DAPI (1:5000) in PBS at room temperature for 1 hr. Afterwards, samples were washed (2x) and kept in PBS at 4°C until imaged with a Zeiss 710 confocal microscope (Zeiss, Munich, Germany). All Alexa Fluor reagents were bought from Life Technologies (Grand Island, NY).

3.3. Labeled fibronectin

To FRET-label, Fn was semi-randomly labeled with Alexa Fluor 546 maleimide and Alexa Fluor 488 succinimidyl ester, as previously described [6]. To single-label, Fn was randomly labeled with Alexa Fluor 633 succinimidyl ester [27].

3.4. FRET-Fn imaging

Assembled FRET-Fn were imaged with a Zeiss 710 confocal. 16-bit Z-stack images spaced 2 μm apart, were obtained with the C-apochromat water-immersion 40×/1.2 objective, a pinhole of 2 AU, a 488 nm laser set at 10% power, and a pixel dwell time of 6.3 μs. FRET-Fn fluorescence was collected to quantify FRET ratios (defined as intensity ratios of

acceptor and donor fluorophores = I_A/I_D) for Fn conformation. Representative z-stack images were stacked in ImageJ (NIH).

3.5. Quantification of VEGF immobilization to Fn matrix

Ratiometric images of VEGF on Fn fibers were also obtained on the confocal, but with z-stack images spaced 1 μm apart. Immunofluorescently-labeled 488-VEGF$_{165}$ was excited with a 488 nm laser set at 10% power, and 633-Fn was excited with a 633 nm laser set at 20% power. Ratios of 488-VEGF$_{165}$/633-Fn were used to quantify VEGF$_{165}$ immobilization onto Fn fibers.

3.6. Time-lapse spinning disk confocal imaging

488-labeled Fn were provided to cultures 24 hrs before Day 1, 5, 8 time points. At each time point, samples were placed in a confined chamber within an Inverted Andor/Olympus IX-83 spinning disk confocal microscope (Olympus Corporation, Tokyo, Japan) and time-lapse z-stack images were taken every 10 min at 4 separate locations per sample for up to 16 hrs past the aforementioned timepoints. Each field of view has an area of 212 μm × 212 μm. Individual fibers were followed over time and changes in length were measured in ImageJ (NIH). Changes in fiber length were fitted to a single exponential decay model:

$\Delta\delta(t) = Ae^{-\frac{t}{\tau}}$; where   δ(t) is the fiber length decay and τ the characteristic time decay.

3.7. Proangiogenic secretion

Media at each time point were collected and centrifuged at 13500 rpm for 15 min at 4°C to collect supernatants free of cell-debris. VEGF secretion was normalized to DNA extracted from the same time point samples in Caron's buffer. Data were represented as ratios to the average 1d control samples of each experiment.

3.8. Statistical analysis

Data were statistically analyzed in GraphPad Prism (GraphPad Software, Inc., CA) with student's t-tests or ANOVAs with Tukey's post-hoc tests and statistical significance was determined at $p < 0.05$. Mean ± SEM.

Supplementary Material

Refer to Web version on PubMed Central for supplementary material.

Acknowledgments

References

1. Lu P, Weaver VM, Werb Z. The extracellular matrix: A dynamic niche in cancer progression. The Journal of Cell Biology. 2012; 196:395–406. DOI: 10.1083/jcb.201102147 [PubMed: 22351925]

2. Jaalouk DE, Lammerding J. Mechanotransduction gone awry. Nat Rev Mol Cell Biol. 2009; 10:63–73. DOI: 10.1038/nrm2597 [PubMed: 19197333]

3. Wang K, Seo BR, Fischbach C, Gourdon D. Fibronectin Mechanobiology Regulates Tumorigenesis. Cell Mol Bioeng. 2016; 9:1–11. DOI: 10.1007/s12195-015-0417-4 [PubMed: 26900407]

4. Stenman S, Vaheri A. Fibronectin in human solid tumors. Int J Cancer. 1981; 27:427–435. [PubMed: 7024140]

5. Chandler EM, Saunders MP, Yoon CJ, Gourdon D, Fischbach C. Adipose progenitor cells increase fibronectin matrix strain and unfolding in breast tumors. Phys Biol. 2011; 8:015008.doi: 10.1088/1478-3975/8/1/015008 [PubMed: 21301062]

6. Wang K, Andresen Eguiluz RC, Wu F, Seo BR, Fischbach C, Gourdon D. Stiffening and unfolding of early deposited-fibronectin increase proangiogenic factor secretion by breast cancer-associated stromal cells. Biomaterials. 2015; 54:63–71. DOI: 10.1016/j.biomaterials.2015.03.019 [PubMed: 25907040]

7. Levental KR, Yu H, Kass L, Lakins JN, Egeblad M, Erler JT, et al. Matrix crosslinking forces tumor progression by enhancing integrin signaling. Cell. 2009; 139:891–906. DOI: 10.1016/j.cell. 2009.10.027 [PubMed: 19931152]

8. Provenzano PP, Inman DR, Eliceiri KW, Knittel JG, Yan L, Rueden CT, et al. Collagen density promotes mammary tumor initiation and progression. BMC Med. 2008; 6:11.doi: 10.1186/1741-7015-6-11 [PubMed: 18442412]

9. Sottile J, Hocking DC. Fibronectin Polymerization Regulates the Composition and Stability of Extracellular Matrix Fibrils and Cell-Matrix Adhesions. Molecular Biology of the Cell. 2002; 13:3546–3559. DOI: 10.1091/mbc.E02 [PubMed: 12388756]

10. McDonald JA, Kelley DG, Broekelmann TJ. Role of fibronectin in collagen deposition: Fab′ to the gelatin-binding domain of fibronectin inhibits both fibronectin and collagen organization in fibroblast extracellular matrix. The Journal of Cell Biology. 1982; 92:485–492. [PubMed: 7061591]

11. Velling T, Risteli J, Wennerberg K, Mosher DF, Johansson S. Polymerization of type I and III collagens is dependent on fibronectin and enhanced by integrins alpha 11beta 1 and alpha 2beta 1. J Biol Chem. 2002; 277:37377–37381. DOI: 10.1074/jbc.M206286200 [PubMed: 12145303]

12. Kubow KE, Vukmirovic R, Zhe L, Klotzsch E, Smith ML, Gourdon D, et al. Mechanical forces regulate the interactions of fibronectin and collagen I in extracellular matrix. Nat Commun. 2015; 6:8026.doi: 10.1038/ncomms9026 [PubMed: 26272817]

13. Eyckmans J, Boudou T, Yu X, Chen CS. Perspective. Developmental Cell. 2011; 21:35–47. DOI: 10.1016/j.devcel.2011.06.015 [PubMed: 21763607]

14. Bradshaw MJ, Smith ML. Multiscale relationships between fibronectin structure and functional properties. Acta Biomaterialia. 2014; 10:1524–1531. DOI: 10.1016/j.actbio.2013.08.027 [PubMed: 23978411]

15. Mouw JK, Ou G, Weaver VM. Extracellular matrix assembly: a multiscale deconstruction. Nat Rev Mol Cell Biol. 2000; 15:771–785. DOI: 10.1038/nrm3902

16. Chen Y, Zardi L, Peters DM. High-resolution cryo-scanning electron microscopy study of the macromolecular structure of fibronectin fibrils. Scanning. 1997; 19:349–355. [PubMed: 9262019]

17. Dallas SL, Sivakumar P, Jones CJP, Chen Q, Peters DM, Mosher DF, et al. Fibronectin regulates latent transforming growth factor-beta (TGF beta) by controlling matrix assembly of latent TGF beta-binding protein-1. J Biol Chem. 2005; 280:18871–18880. DOI: 10.1074/jbc.M410762200 [PubMed: 15677465]

18. Moriya K, Bae E, Honda K, Sakai K, Sakaguchi T, Tsujimoto I, et al. A fibronectin-independent mechanism of collagen fibrillogenesis in adult liver remodeling. Gastroenterology. 2011; 140:1653–1663. DOI: 10.1053/j.gastro.2011.02.005 [PubMed: 21320502]

19. Ledger PW, Uchida N, Tanzer ML. Immunocytochemical localization of procollagen and fibronectin in human fibroblasts: effects of the monovalent ionophore, monensin. The Journal of Cell Biology. 1980; 87:663–671. [PubMed: 7007394]

20. Erat MC, Sladek B, Campbell ID, Vakonakis I. Structural analysis of collagen type I interactions with human fibronectin reveals a cooperative binding mode. Journal of Biological Chemistry. 2013; 288:17441–17450. DOI: 10.1074/jbc.M113.469841 [PubMed: 23653354]

21. Janmey PA, Miller RT. Mechanisms of mechanical signaling in development and disease. Journal of Cell Biology. 2011; 124:9–18. DOI: 10.1242/jcs.071001

22. Ma X, Schickel ME, Stevenson MD, Sarang-Sieminski AL, Gooch KJ, Ghadiali SN, et al. Fibers in the Extracellular Matrix Enable Long-Range Stress Transmission between Cells. Biophysical Journal. 2013; 104:1410–1418. DOI: 10.1016/j.bpj.2013.02.017 [PubMed: 23561517]

23. Shen ZL, Kahn H, Ballarini R, Eppell SJ. Viscoelastic Properties of Isolated Collagen Fibrils. Biophysical Journal. 2011; 100:3008–3015. DOI: 10.1016/j.bpj.2011.04.052 [PubMed: 21689535]

24. Klotzsch E, Smith ML, Kubow KE, Muntwyler S, Little WC, Beyeler F, et al. Fibronectin forms the most extensible biological fibers displaying switchable force-exposed cryptic binding sites. Proc Natl Acad Sci USa. 2009; 106:18267–18272. DOI: 10.1073/pnas.0907518106 [PubMed: 19826086]

25. Hubbard B, Buczek-Thomas JA, Nugent MA, Smith ML. Fibronectin Fiber Extension Decreases Cell Spreading and Migration. J Cell Physiol. 2015; n/a–n/a. doi: 10.1002/jcp.25271

26. Ohashi T, Kiehart DP, Erickson HP. Dynamics and elasticity of the fibronectin matrix in living cell culture visualized by fibronectin-green fluorescent protein. Proc Natl Acad Sci USa. 1999; 96:2153–2158. [PubMed: 10051610]

27. Hynes RO. The dynamic dialogue between cells and matrices: implications of fibronectin's elasticity. Proc Natl Acad Sci USa. 1999; 96:2588–2590. [PubMed: 10077553]

28. Smith ML, Gourdon D, Little WC, Kubow KE, Eguiluz RA, Luna-Morris S, et al. Force-Induced Unfolding of Fibronectin in the Extracellular Matrix of Living Cells. Plos Biol. 2007; 5:e268.doi: 10.1371/journal.pbio.0050268.sv001 [PubMed: 17914904]

29. Kubow KE, Klotzsch E, Smith ML, Gourdon D, Little WC, Vogel V. Crosslinking of cell-derived 3D scaffolds up-regulates the stretching and unfolding of new extracellular matrix assembled by reseeded cells. Integr Biol (Camb). 2009; 1:635–648. DOI: 10.1039/b914996a [PubMed: 20027372]

30. Dallas SL, Chen Q, Sivakumar P. Dynamics of assembly and reorganization of extracellular matrix proteins. Curr Top Dev Biol. 2006; 75:1–24. DOI: 10.1016/S0070-2153(06)75001-3 [PubMed: 16984808]

31. Hu Y, Suo Z. Viscoelasticity and poroelasticity in elastomeric gels. Acta Mechanica Solida Sinica. 2012; 25:441–458. DOI: 10.1016/S0894-9166(12)60039-1

32. McKeown-Longo PJ, Mosher DF. Interaction of the 70,000-mol-wt amino-terminal fragment of fibronectin with the matrix-assembly receptor of fibroblasts. The Journal of Cell Biology. 1985; 100:364–374. [PubMed: 3155749]

33. Früh SM, Schoen I, Ries J, Vogel V. Molecular architecture of native fibronectin fibrils. Nat Commun. 2015; 6:7275.doi: 10.1038/ncomms8275 [PubMed: 26041410]

34. Mao Y, Schwarzbauer JE. Fibronectin fibrillogenesis, a cell-mediated matrix assembly process. Matrix Biology. 2005; 24:389–399. DOI: 10.1016/j.matbio.2005.06.008 [PubMed: 16061370]

35. Swartz MA, Fleury ME. Interstitial Flow and Its Effects in Soft Tissues. Annu Rev Biomed Eng. 2007; 9:229–256. DOI: 10.1146/annurev.bioeng.9.060906.151850 [PubMed: 17459001]

36. Mak AF. The apparent viscoelastic behavior of articular cartilage--the contributions from the intrinsic matrix viscoelasticity and interstitial fluid flows. J Biomech Eng. 1986; 108:123–130. [PubMed: 3724099]

37. Bloom RJ, George JP, Celedon A, Sun SX, Wirtz D. Mapping Local Matrix Remodeling Induced by a Migrating Tumor Cell Using Three-Dimensional Multiple-Particle Tracking. Biophysical Journal. 2008; 95:4077–4088. DOI: 10.1529/biophysj.108.132738 [PubMed: 18641063]

38. Pedersen JA, Swartz MA. Mechanobiology in the third dimension. Ann Biomed Eng. 2005; 33:1469–1490. DOI: 10.1007/s10439-005-8159-4 [PubMed: 16341917]

39. Netti PA, Berk DA, Swartz MA, Grodzinsky AJ, Jain RK. Role of extracellular matrix assembly in interstitial transport in solid tumors. 2000; 60:2497–2503.

40. Guidry C, Grinnell F. Contraction of hydrated collagen gels by fibroblasts: evidence for two mechanisms by which collagen fibrils are stabilized. Collagen and Related Research. 1987; 6:515–529. http://eutils.ncbi.nlm.nih.gov/entrez/eutils/elink.fcgi?dbfrom=pubmed&id=3581756&retmode=ref&cmd=prlinks. [PubMed: 3581756]

41. Raeber GP, Lutolf MP, Hubbell JA. Molecularly Engineered PEG Hydrogels: A Novel Model System for Proteolytically Mediated Cell Migration. Biophysical Journal. 2005; 89:1374–1388. DOI: 10.1529/biophysj.104.050682 [PubMed: 15923238]

42. Egeblad M, Werb Z. New functions for the matrix metalloproteinases in cancer progression. Nat Rev Cancer. 2002

43. Oskarsson T. Extracellular matrix components in breast cancer progression and metastasis. The Breast. 2013; 22:S66–S72. DOI: 10.1016/j.breast.2013.07.012 [PubMed: 24074795]

44. Grant MB, Caballero S, Bush DM, Spoerri PE. Fibronectin fragments modulate human retinal capillary cell proliferation and migration. Diabetes. 1998; 47:1335–1340. [PubMed: 9703336]

45. Kessenbrock K, Plaks V, Werb Z. Matrix Metalloproteinases: Regulators of the Tumor Microenvironment. Cell. 2010; 141:52–67. DOI: 10.1016/j.cell.2010.03.015 [PubMed: 20371345]

46. Zhang X, Chen CT, Bhargava M, Torzilli PA. A Comparative Study of Fibronectin Cleavage by MMP-1, -3, -13, and -14. Cartilage. 2012; 3:267–277. DOI: 10.1177/1947603511435273 [PubMed: 26069638]

47. Shi F, Sottile J. MT1-MMP regulates the turnover and endocytosis of extracellular matrix fibronectin. Journal of Cell Biology. 2011; 124:4039–4050. DOI: 10.1242/jcs.087858

48. Manka SW, Carafoli F, Visse R, Bihan D, Raynal N, Farndale RW, et al. Structural insights into triple-helical collagen cleavage by matrix metalloproteinase 1. Proc Natl Acad Sci USa. 2012; 109:12461–12466. DOI: 10.1073/pnas.1204991109 [PubMed: 22761315]

49. Malik R, Lelkes PI, Cukierman E. Biomechanical and biochemical remodeling of stromal extracellular matrix in cancer. Trends Biotechnol. 2015; 33:230–236. DOI: 10.1016/j.tibtech.2015.01.004 [PubMed: 25708906]

50. Lee HO, Mullins SR, Franco-Barraza J, Valianou M, Cukierman E, Cheng JD. FAP-overexpressing fibroblasts produce an extracellular matrix that enhances invasive velocity and directionality of pancreatic cancer cells. BMC Cancer. 2011; 11:1.doi: 10.1186/1471-2407-11-245 [PubMed: 21194487]

51. Bergers G, Brekken R, McMahon G, Vu TH, Itoh T, Tamaki K, et al. Matrix metalloproteinase-9 triggers the angiogenic switch during carcinogenesis. Nature Cell Biology. 2000; 2:737–744. DOI: 10.1038/35036374 [PubMed: 11025665]

52. Lee S, Jilani SM, Nikolova GV, Carpizo D, Iruela-Arispe ML. Processing of VEGF-A by matrix metalloproteinases regulates bioavailability and vascular patterning in tumors. The Journal of Cell Biology. 2005; 169:681–691. DOI: 10.1083/jcb.200409115 [PubMed: 15911882]

53. Sottile J, Hocking DC, Langenbach KJ. Fibronectin polymerization stimulates cell growth by RGD-dependent and -independent mechanisms. Journal of Cell Biology. 2000; 113(Pt 23):4287–4299.

54. Martino MM, Hubbell JA. The 12th-14th type III repeats of fibronectin function as a highly promiscuous growth factor-binding domain. The FASEB Journal. 2010; 24:4711–4721. DOI: 10.1096/fj.09-151282 [PubMed: 20671107]

55. Chen TT, Luque A, Lee S, Anderson SM, Segura T, Iruela-Arispe ML. Anchorage of VEGF to the extracellular matrix conveys differential signaling responses to endothelial cells. The Journal of Cell Biology. 2010; 188:595–609. DOI: 10.1083/jcb.200906044.dv [PubMed: 20176926]

56. Park JE, Keller GA, Ferrara N. The vascular endothelial growth factor (VEGF) isoforms: differential deposition into the subepithelial extracellular matrix and bioactivity of extracellular matrix-bound VEGF. Molecular Biology of the Cell. 1993; 4:1317–1326. [PubMed: 8167412]

57. Senger DR, Claffey KP, Benes JE, Perruzzi CA, Sergiou AP, Detmar M. Angiogenesis promoted by vascular endothelial growth factor: regulation through alpha1beta1 and alpha2beta1 integrins. Proc Natl Acad Sci USa. 1997; 94:13612–13617. http://eutils.ncbi.nlm.nih.gov/entrez/eutils/elink.fcgi?dbfrom=pubmed&id=9391074&retmode=ref&cmd=prlinks. [PubMed: 9391074]

58. Wijelath ES, Murray J, Rahman S, Patel Y, Ishida A, Strand K, et al. Novel vascular endothelial growth factor binding domains of fibronectin enhance vascular endothelial growth factor biological activity. Circulation Research. 2002; 91:25–31. DOI: 10.1161/01.RES. 0000026420.22406.79 [PubMed: 12114318]

59. De S, Razorenova O, McCabe NP, O'Toole T, Qin J, Byzova TV. VEGF-integrin interplay controls tumor growth and vascularization. Proc Natl Acad Sci USa. 2005; 102:7589–7594. DOI: 10.1073/pnas.0502935102 [PubMed: 15897451]

60. Hubbard B, Buczek-Thomas JA, Nugent MA, Smith ML. Heparin-dependent regulation of fibronectin matrix conformation. Matrix Biol. 2013; 34:124–131. DOI: 10.1016/j.matbio.2013.10.006 [PubMed: 24148804]

Highlights

- Breast cancer cells recruit stromal cells to alter ECM remodeling

- Tumor-associated fibronectin matrix is remodeled into a thick Col I-rich matrix

- Tumor-associated MMP activity leads to structural and mechanical ECM alterations

- Tumor-mediated alterations of the ECM dysregulate its proangiogenic activity

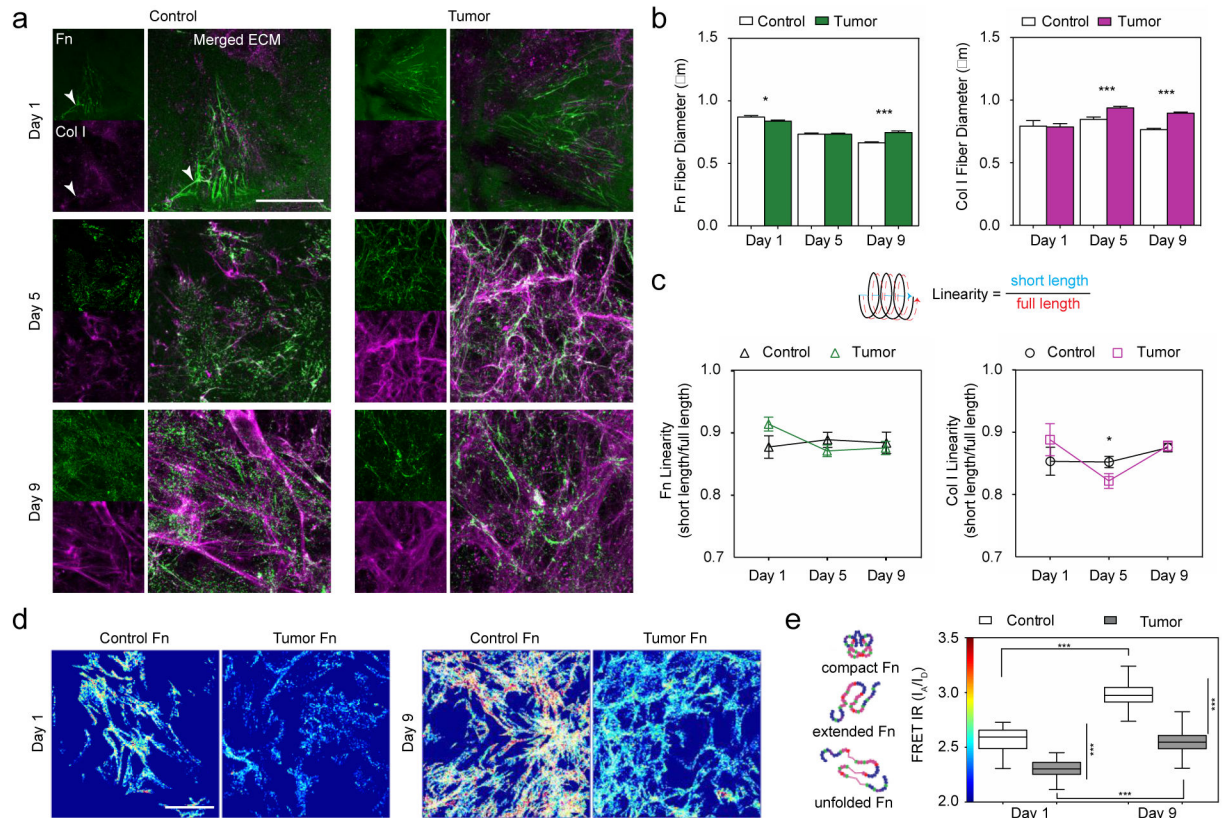- Fibronectin and collagen I cooperate to promote breast tumorigenesis

Figure 1. Structural and conformational alterations in the developing tumor-associated (TC) Fn-Col I matrix

a) Immunofluorescence depicting the evolution of control (c)- and tumor-associated (TC)-ECMs over 9 days: fibronectin (green) and collagen I (magenta). Overlay of ECM with F-actin and DAPI is shown in SI Fig 1. While Fn is present at all times, fibrillar Col I is only fully assembled at later time points.

b) TC- fibers (both Fn and Col I) become gradually thicker than their control (c-) counterparts. **Fn** Day 1: 0.84 ± 0.01 μm, n = 723 vs. 0.87 ± 0.01 μm, n = 640; $p < 0.05$. **Col I** Day 1: 0.79 ± 0.03 μm, n = 66 vs. 0.79 ± 0.04 μm, n = 54. **Fn** Day 5: 0.73 ± 0.01 μm, n = 1862 vs. 0.73 ± 0.01 μm, n = 1226. **Col I** Day 5: 0.94 ± 0.01 μm, n = 432 vs. 0.84 ± 0.02 μm, n = 338; $p < 0.0001$. **Fn** Day 9: 0.75 ± 0.01 μm, n = 1337 vs. 0.66 ± 0.01 μm, n = 1012. **Col I** Day 9: 0.9 ± 0.01 μm, n = 1297 vs. 0.76 ± 0.01 μm, n = 647; $p < 0.0001$. Mean ± SEM.

c) Although TC- fibers (both Fn and Col I) are initially more strained (higher linearity) than c- fibers, all data converge towards a similar steady-state strain value in the mature ECM. **Fn** Day 1: 0.91 ± 0.01, n = 90 vs. 0.88 ± 0.02, n = 49. **Col I** Day 1: 0.89 ± 0.03, n = 34 vs. 0.85 ± 0.02, n = 31. **Fn** Day 5: 0.87 ± 0.01, n = 130 vs. 0.89 ± 0.01, n = 79; **Col I** Day 5: 0.82 ± 0.01, n = 169 vs. 0.85 ± 0.01, n = 200; $p < 0.05$. **Fn** Day 9: 0.88 ± 0.01, n = 92 vs. 0.88 ± 0.02, n = 38; **Col I** Day 9: 0.88 ± 0.01, n = 205 vs. 0.88 ± 0.01, n = 220. Mean ± SEM.

d) FRET maps show lower FRET, i.e., more unfolded Fn, in TC-ECM (bluish fibers) than in c-ECM (yellow/red fibers). Scale bar: 50 μm.

e) Mean FRET ratios (I_A/I_D) highlight the significant conformational differences between TC-Fn and c-Fn and their evolution over time. **FRET** Day 1: 2.303 ± 0.011, n = 47 vs. 2.566 ± 0.013, n = 54; $p < 0.0001$. FRET maps also display a global shift towards higher FRET from Day 1 to Day 9, indicating Fn fiber relaxation in presence of Col I. **FRET** Day 9: 2.552 ± 0.013, n = 60 vs. 2.975 ± 0.012, n = 76; $p < 0.0001$. Mean $\pm$ SEM.
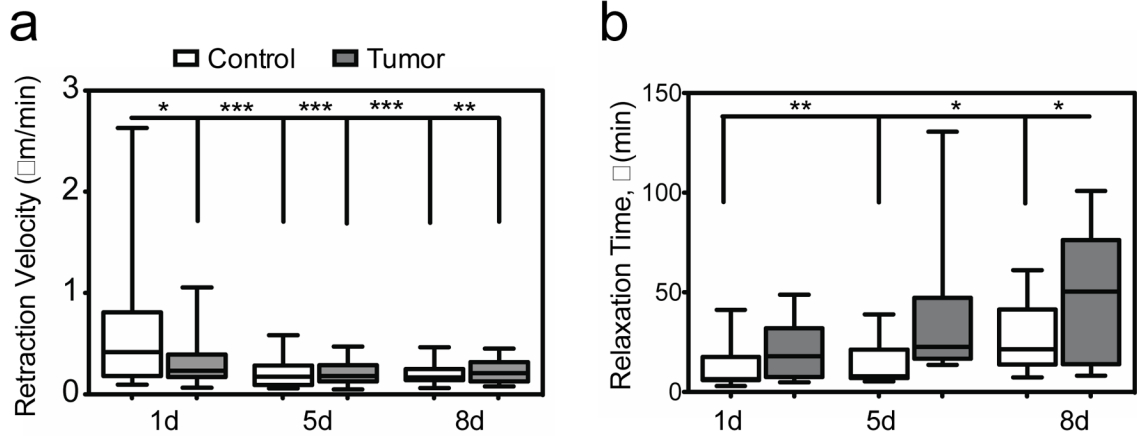
Figure 2. Viscoelastic alterations in individual TC-Fn fibers (See SI movies)

a) During remodeling, mean retraction velocities of Fn fibers decrease over time and tend to be smaller in TC- than in c- samples. TC-Fn: Day 1 = 0.33 ± 0.05 μm/min, n = 26; $p < 0.05$. Day 5 = 0.21 ± 0.02 μm/min, n = 22; $p < 0.0001$. Day 8 = 0.22 ± 0.03, n = 13; $p < 0.001$; c-Fn: Day 1 = 0.57 ± 0.1 μm/min, n = 30. Day 5 = 0.2 ± 0.03 μm/min, n = 24; $p < 0.0001$. Day 8 = 0.21 ± 0.02 μm/min, n = 21; $p < 0.0001$. Mean ± SEM.

b) Determined from fitting fiber length decay to a single exponential model, relaxation times, τ (min), increase over time and are significantly longer in TC- fibers than in c- fibers, highlighting overall slower responses of TC- Fn fibers. TC-Fn: Day 1 = 21.8 ± 4.9 min, n = 11. Day 5 = 38.9 ± 11.7 min, n = 10. Day 8 = 45.4 ± 16.8 min, n = 5; $p < 0.05$. c-Fn: Day 1 = 11.5 ± 3.4 min, n = 11; Day 5 = 14.3 ± 4.6 min, n = 7; $p < 0.01$. Day 8 = 26.8 ± 4.7 min, n = 12; ; $p < 0.05$. Mean ± SEM.
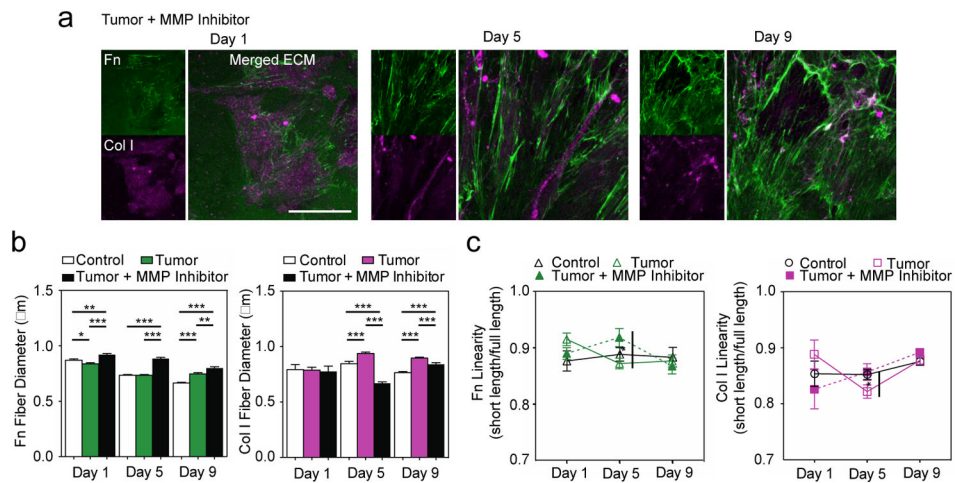
Figure 3. Role of matrix metalloproteinases (MMP) in alterations of TC-matrix remodeling

a) Immunofluorescence of MMP inhibited (MI/) TC-ECMs reveals a predominantly Fn matrix and very few Col I fibers. Scale bar: 50 μm.

b) MI/TC-Fn fibers are thicker than c- and TC-Fn fibers, while the sparse MI/TC-Col I fibers are much thinner than TC-Col fibers. **Fn** Day 1: 0.92 ± 0.01 μm, n = 732; $p < 0.01$ (c-Fn); $p < 0.0001$ (TC-Fn), Day 5: 0.88 ± 0.01 μm, n = 811; $p < 0.0001$ (c-Fn & TC-Fn), Day 9: 0.8 ± 0.01 μm, n = 1078; $p < 0.0001$ (c-Fn); $p < 0.01$ (TC-Fn)). **Col I** Day 1: 0.78 ± 0.05 μm, n = 33, Day 5: 0.67 ± 0.01 μm, n = 232; $p < 0.0001$ (c-Fn & TC-Fn), Day 9: 0.84 ± 0.01 μm, n = 383; $p < 0.0001$ (c-Fn); $p < 0.001$ (TC-Fn). Mean ± SEM.

c) MI/TC-Fn linearity indicates a significant maximum in Fn strain at Day 5. MI/TC-Col I linearity gradually increases with time. Linearity of MI/ fibers (for both Fn and Col I) converges towards the same steady-state strain value similar to that of c- and TC- mature fibers at Day 9. **Fn** Day 1: Day 1: 0.89 ± 0.01, n = 94, Day 5: 0.92 ± 0.02, n = 55; $p < 0.05$, Day 9: 0.87 ± 0.01, n = 76. ; **Col I** Day 1: 0.83 ± 0.03, n = 14, Day 5: 0.86 ± 0.01, n = 90, Day 9: 0.89 ± 0.01, n = 130. Mean ± SEM.
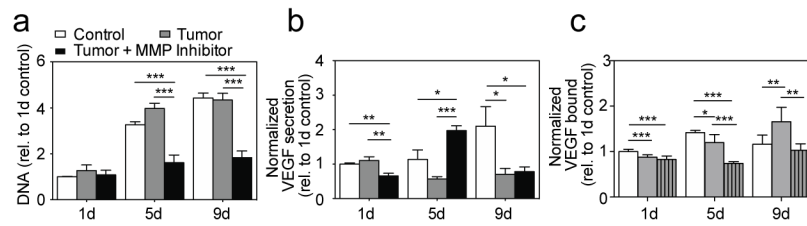
Figure 4. Fluctuations of pro-angiogenic activity during TC-matrix remodeling

a) TC-DNA is similar to c-DNA. Day 1: 1.27 ± 0.24, n = 6 vs. 1 ± 0.024, n = 6; Day 5: 3.97 ± 0.23, n = 6 vs. 3.26 ± 0.14, n = 6; Day 9: 4.34 ± 0.295, n = 6 vs. 4.43 ± 0.21, n= 5. MI/TC-DNA is significantly lower than TC-DNA at later time points, indicating that fewer cells attach to MMP-inhibited Fn-rich matrices. MI/TC-DNA Day 1: 1.08 ± 0.21, n = 6, MI/TC-DNA Day 5: 1.61 ± 0.34, n = 6; $p < 0.0001$ (TC-ECM & MI/TC-ECM), MI/TC-DNA Day 9: 1.84 ± 0.29, n = 6 vs. 4.34 ± 0.295, n = 6; $p < 0.001$ (TC-ECM & MI/TC-ECM). Mean $\pm$ SEM.

b) Over time, TC-VEGF secretion (normalized to DNA, then to 1d control) decreases, while MI/TC-VEGF secretion reaches a maximum at Day 5, when CAFs interact with a highly stretched/unfolded Fn-rich matrix. Day 1: 1.11 ± 0.11, n = 6 vs. 1 ± 0.03, n = 6, Day 5: 0.57 ± 0.06, n = 6 vs. 1.13 ± 0.28, n = 6, Day 9: 0.70 ± 0.18, n = 6 vs. 2.10 ± 0.56, n = 5; $p < 0.05$ (TC-ECM & c-ECM)). MI/TC-ECM Day 1: 0.66 ± 0.073, n = 6; $p < 0.01$ (c- & TC-ECM), MI/TC-ECM Day 5: 1.97 ± 0.15, n = 6; $p < 0.05$ (c-ECM); $p < 0.0001$ (TC-ECM), MI/TC-ECM Day 9: 0.78 ± 0.14, n = 6; $p < 0.05$ (c-ECM). Mean $\pm$ SEM.

c) Analysis of $VEGF_{165}$ immobilization (normalized to Fn, with respect to 1d control) reveals that, although less VEGF binds to stretched/unfolded TC-Fn fibers (Day 1 and Day 5), TC-VEGF sequestration increases over time, which could partly explain the simultaneous decrease of soluble VEGF levels detected in TC samples (panel b). Day 1: 0.88 ± 0.02, n=7 vs. 1 ± 0.02, n = 7; $p < 0.001$, Day 5: 1.20 ± 0.08, n = 5 vs. 1.42 ± 0.02, n = 5; $p < 0.05$, Day 9: 1.66 ± 0.13, n = 6 vs. 1.16 ± 0.08, n = 6; $p < 0.01$ (TC-ECM & c-ECM)). MI/TC-ECM Day 1: 0.82 ± 0.03, n = 7; $p < 0.001$ (c-ECM), MI/TC-ECM Day 5: 0.74 ± 0.01, n = 6; $p < 0.001$ (c-ECM); $p < 0.001$ (TC-ECM), MI/TC-ECM Day 9: 1.02 ± 0.06, n = 6; $p < 0.01$ (TC-ECM). Mean $\pm$ SEM.